

---

*Research Article: New Research | Sensory and Motor System*

## Large-Scale Networks for Auditory Sensory Gating in the awake mouse

<https://doi.org/10.1523/ENEURO.0207-19.2019>

**Cite as:** eNeuro 2019; 10.1523/ENEURO.0207-19.2019

Received: 31 May 2019

Revised: 28 June 2019

Accepted: 1 July 2019

---

*This Early Release article has been peer-reviewed and accepted, but has not been through the composition and copyediting processes. The final version may differ slightly in style or formatting and will contain links to any extended data.*

**Alerts:** Sign up at [www.eneuro.org/alerts](http://www.eneuro.org/alerts) to receive customized email alerts when the fully formatted version of this article is published.

Copyright © 2019 Khani et al.

This is an open-access article distributed under the terms of the Creative Commons Attribution 4.0 International license, which permits unrestricted use, distribution and reproduction in any medium provided that the original work is properly attributed.



## 1 **Abstract**

2           The amplitude of the brain response to a repeated auditory stimulus is diminished as  
3 compared to the response to the first tone (T1) for interstimulus intervals (ISI) lasting up to  
4 hundreds of milliseconds. This adaptation process, called auditory sensory gating (ASG), is  
5 altered in various psychiatric diseases including schizophrenia and is classically studied by  
6 focusing on early evoked cortical responses to the second tone (T2) using 500 ms ISI.  
7 However, mechanisms underlying ASG are still not well-understood. We investigated ASG in  
8 awake mice from the brainstem to cortex at variable ISIs (125-2000 ms) using high-density  
9 EEG and intracerebral recordings. While ASG decreases at longer ISIs, it is still present at  
10 durations (500-2000 ms) far beyond the time during which brain responses to T1 could still be  
11 detected. T1 induces a sequence of specific stable scalp EEG topographies that correspond to  
12 the successive activation of distinct neural networks lasting about 350 ms. These brain states  
13 remain unaltered if T2 is presented during this period, although T2 is processed by the brain,  
14 suggesting that ongoing networks of brain activity are active for longer than early evoked-  
15 potentials and are not overwritten by an upcoming new stimulus. Intracerebral recordings  
16 demonstrate that ASG is already present at the level of ventral cochlear nucleus and inferior  
17 colliculus and is amplified across the hierarchy in bottom-up direction. This study uncovers  
18 the extended stability of sensory-evoked brain states and long duration of ASG, and sheds  
19 light on generators of ASG and possible interactions between bottom-up and top-down  
20 mechanisms.

21

22 **Keywords;** Auditory cortex, sensory gating, large-scale networks, brain state, EEG, cochlear  
23 nucleus, inferior colliculus, anterior cingulate cortex, paired tone

24 **Significance**

25 Stimulus-evoked responses of neurons fade rapidly and last usually up to around 100 ms in  
26 small brains such as the mice brain. The brain also attenuates the response to the second of a  
27 pair of stimuli (e.g. auditory), a phenomenon that is called sensory gating (SG) and is  
28 impoverished in schizophrenia patients. Here, first, we demonstrate that SG is present in  
29 ventral cochlear nucleus, the first station of auditory pathway in the CNS, and is  
30 hierarchically organized such that SG is amplified as the signal travels from early brain  
31 regions to higher order processing areas. Second, we show that brain networks are active for  
32 longer than early evoked-potentials highlighting the importance of often-neglected late  
33 components of brain response to sensory stimuli.

## 34 **Introduction**

35 In the auditory system, a single repetition of a tone is enough for the brain to diminish the  
36 amplitude of the neural response to the second tone. This adaptive property, called auditory  
37 sensory gating (ASG), has been detected in many brain regions in human and animals  
38 including auditory cortices (Grunwald et al., 2003; Wehr and Zador, 2005; Kurthen et al.,  
39 2007; Mayer et al., 2009), prefrontal areas (Alho et al., 1994; Mears et al., 2006; Williams et  
40 al., 2011), parietal areas (Grunwald et al., 2003; Knott et al., 2009), amygdala (Cromwell et  
41 al., 2005) and hippocampus (Grunwald et al., 2003; Witten et al., 2016). In previous works  
42 (Brosch and Schreiner, 1997; Wehr and Zador, 2005), forward masking, forward inhibition  
43 and two-tone interaction have almost interchangeably been used to describe sensory gating or  
44 very similar phenomena. Sensory gating is thought to be a fundamental mechanism that  
45 contributes to information processing by filtering extraneous sensory inputs (Qi et al., 2015),  
46 by minimizing surprise based on sensory inputs prediction (Rao and Ballard, 1999; Friston,  
47 2018; Giraud and Arnal, 2018) or by serving as an energy saving system since the brain must  
48 adopt energy efficient mechanisms (Niven and Laughlin, 2008). Impairment in neuronal  
49 adaptation to successively presented auditory stimuli is manifest in schizophrenia patients and  
50 may represent a core physiologic dysfunction (Adler et al., 1982; Grunwald et al., 2003; Javitt  
51 and Sweet, 2015).

52 Several mechanisms may be responsible for ASG, from local short-term synaptic mechanisms  
53 in the auditory cortices (Wehr and Zador, 2005; Christianson et al., 2011) to larger-scale  
54 bottom-up or top-down modulations, and these mechanisms may act at different time-scales in  
55 the course of different durations of the ISI. Ascending projections from brainstem reticular  
56 neurons to the medial septal nucleus have been proposed as a bottom-up mechanism that  
57 would promote inhibition in the hippocampus, thalamus and neocortex (Javitt and Freedman,  
58 2015). On the other hand, top-down mechanisms have been hypothesized in which ASG

59 would be modulated by corticofugal projections to reticular thalamus inhibitory circuits (Yu  
60 et al., 2004; Duque et al., 2014) or by inhibitory modulations in auditory cortices projecting  
61 from the prefrontal cortex (Alho et al., 1994; Grunwald et al., 2003; Mears et al., 2006;  
62 Williams et al., 2011). Still, as simple the ASG phenomenon may seem, the neural correlates  
63 of ASG and especially its connections to higher order brain functions remain poorly  
64 understood.

65 In which brain region within the auditory network is ASG first detectable? How long after the  
66 first tone (T1) is the response to the second tone (T2) still gated? What are the differences  
67 between ASG following short and long ISIs in local brain areas and global brain states? As  
68 yet, we do not have clear responses to these questions. Indeed, most ASG studies used a  
69 single inter-stimulus interval (ISI) of 500 ms and focused their analyses on specific surface  
70 EEG components or on early stimulus-evoked responses in local brain areas. For a better  
71 understanding of the mechanisms underpinning ASG, three points are important to be  
72 considered. First, we must study the dynamics of ASG in human and in awake animal models  
73 from short to long ISI as the adaptive mechanisms may be different for different ISI durations.  
74 Second, the effects of auditory stimuli and ASG should be examined beyond the initial  
75 evoked response, i.e. further during the ISI. Finally, ASG should be studied at large-scale  
76 level as auditory stimuli activate a large set of neural networks and we hypothesized that they  
77 potentially exert a profound influence across the entire brain by modifying the global brain  
78 state.

79 In the present work, we therefore systematically characterized the effects of ASG using a  
80 paired-tone paradigm with variable ISIs (125-2000 ms) and recorded brain responses of  
81 awake mice at a large-scale level with high-density EEG and intracerebral electrodes in  
82 multiple brain areas ranging from as early as ventral cochlear nucleus (vCN) to higher-order  
83 brain areas (anterior cingulate cortex; ACC). We also studied the effect of auditory and ASG

- 84 processing at the level of brain states using clustering analyses of surface voltage
- 85 topographies and pre-T2 brain activity recorded intracerebrally from multiple brain regions.

## 86 **Materials and Methods**

87

### 88 **Animals**

89 Twenty-six male C57BL/6J mice (2-3 months old; Charles River), were recorded in this  
90 study. We recorded epicranial EEG in seven mice (3 to 5 recording sessions per animal,  
91 population statistics were performed across subjects). Intracranial recordings were performed  
92 in 19 mice. One to three recording sessions from different brain regions were accomplished in  
93 each animal. In a few cases, a similar brain region was recorded twice in two different  
94 recording sessions but in slightly different sites. Population analyses are based on the number  
95 of recording sites. All experiments were in accordance with the applicable Swiss and  
96 European regulations on animal experimentation and were approved by the Ethics Committee  
97 on Animal Experimentation of the University of Geneva and the Veterinary Office of Canton  
98 of Geneva.

99

### 100 **Surgery**

101 The animals were anesthetized in an induction box with a 2.5% isoflurane and were mounted  
102 in a stereotaxic frame with continuous delivery of 1-1.5% isoflurane to maintain the  
103 anesthesia. Artificial tears ophthalmic gel (lacryvisc; Alcon) was used to avoid corneal  
104 drying and the body temperature was monitored through a rectal probe connected to a closed  
105 loop heating pad. An incision was made on the skin and the skin was retracted. Subsequently,  
106 the positions of epicranial electrodes or intracranial electrode entry points were marked with  
107 ink. The skull was covered by a layer of glue (Loctite; Henkel). Once the glue was dried, a  
108 small patch with a diameter of around 500  $\mu\text{m}$  was removed at each electrode location. A

109 ring-like head-holder was fixed on the occipital and nasal bones using dental cement  
110 (Kaladent AG). The center of the ring was filled with silicon sealant (Kwik-Cast, World  
111 Precision Instrument). Animals were returned to their cage (single-housed post-surgery) and  
112 antibiotics (trimethoprim-sulfamethoxazole, Roche) and nonsteroidal anti-inflammatory and  
113 analgesic medicines (Ibuprofene, Vifor, and Paracetamol, Bristol-Myers) were added to their  
114 drinking water. The animals were allowed to recover from the surgery for at least three days  
115 before the training started.

116

### 117 **Training**

118 The mice were positioned on a stereotaxic frame equipped to head-fix the animals using the  
119 head-posts on their head. The training was continued twice a day for three days preceding the  
120 recording day. Acoustic stimuli were synthesized digitally using Real-Time Processor Visual  
121 Design Studio (RPvdsEx v88, Tucker-Davis Technologies, Alachua, USA) and were  
122 generated by a RZ6 processor (Tucker-Davis Technologies, USA). Calibration of the setup  
123 was performed by measuring the sound pressure level (SPL) emitted by the speaker when  
124 driven by the wideband noise. The animals learned to stay still while paired-tone paradigm  
125 presented pairs of tones (wideband noise; 0.1-12.5 KHz) separated by a variable ISI (62.5,  
126 125, 250, 500, 1000 and 2000 ms). The stimuli were noise bursts of 10 ms long including a 3  
127 ms rise and a 3 ms fall and were presented from a frontal speaker (Electrostatic Loudspeaker,  
128 ES1, Tucker-Davis Technologies, Alachua, USA) positioned at 20cm distance from the center  
129 of the head. The ISI of 62.5 ms was not analyzed here as it was too short epoch for the most  
130 of analysis in the present study. The sound intensity, delivered from our calibrated sound  
131 system, was started at 40 dB and was increased on successive sessions of training until it  
132 reached 70 dB on the last day of training. This intensity was then used during every recording

133 session. An intertrial interval between 8-12 seconds separated each pair of tones ensuring no  
134 remaining brain activity from the preceding trials at the beginning of each trial.

135

### 136 **Epicranial and intracranial electrophysiological recordings**

137 The details of surface recordings were described previously (Megevand et al., 2008;  
138 Quairiaux et al., 2010). Briefly, the mice were anesthetized lightly for a short period and a  
139 grid of epicranial electrodes (32 electrodes) was lowered and adjusted to contact points on the  
140 skull (Fig. 1A). The brief anesthesia ensured precise adjustment of electrode tips such that  
141 they all have direct contact with the skull. The electrode tips were immersed in EEG paste  
142 (EC2, Grass Technologies) before contacting the skull yielding a final impedance of  
143 approximately 50 K $\Omega$ . For intracranial recordings, an A16 probe (NeuroNexus) was  
144 positioned above the surface of brain at entry point and was lowered gently until it reaches the  
145 desired depth. Following anteroposterior (AP), mediolateral (ML) and dorsoventral (DV)  
146 coordinates relative to bregma, midline and surface plane tangent to bregma were used for  
147 these recordings according to a mouse brain atlas (Paxinos and Franklin, 2004), respectively: -  
148 5.20, 1, 2.25 for ICc; -2.7, 4, 2.6 for Au1; and 1.3, 0.2, 2.4 for ACC. All recordings were  
149 performed from the right hemisphere and electrodes were laterally positioned such that a  
150 lateromedial angle of 20° guides the probe to the desired target. After the positioning of the  
151 surface grid or intracranial probes, the light anesthesia was removed and the animals were  
152 allowed to completely wake up before the recording starts. Usually, the animals woke up  
153 within less than five minutes but an additional 15 minutes were allowed to avoid any effect of  
154 anesthesia on recordings. Paired-tone paradigm was run at the beginning of each recording  
155 session. A Digital Lynx SX (Neuralynx) data acquisition system was used for recording both  
156 surface and intracranial recordings. Sampling rates of 4 KHz (low-pass: 2 KHz) and 16 KHz

157 (low-pass: 8 KHz) were used for surface and intracerebral recordings respectively. In order to  
158 synchronize recordings and acoustic stimuli, digital triggers were received from the real-time  
159 processor RZ6 (Tucker-Davis Technologies, USA) during all recording sessions. A thin  
160 reference pin was implanted in the cerebellum of the opposite hemisphere compared to  
161 recording site.

162

### 163 **Data analysis**

164 Data analysis was performed using the Cartool software (D. Brunet, Center for Biomedical  
165 Imaging, University of Geneva, Switzerland (Brunet et al., 2011)) and custom-written Matlab  
166 functions. In this manuscript, AEP refers to auditory evoked potentials in general, eAEP  
167 refers to epicranially recorded AEPs and iAEP refers to intracranially-recorded AEPs, i.e.  
168 drawn from the local field potentials (LFP).

### 169 **Epicranial data analysis**

170 Epicranial data were referenced against an average reference and downsampled to 1 KHz  
171 before any subsequent analysis. Global field power (GFP) is based on the spatial standard  
172 deviation of voltage values at all electrodes and represents the magnitude of activity (potential  
173 field) at a large-scale level (Lehmann and Skrandies, 1980). This measure was calculated  
174 according to the following formula:

$$GFP = \sqrt{\frac{\sum_{i=1}^n (v_i - \bar{v})^2}{n}}$$

175 where  $n$  is the number of electrodes,  $v$  the voltage measured at electrode  $i$  and  $\bar{v}$  is the mean  
176 potential across electrodes. GFP provides a single, positive and reference-free value reflecting  
177 the strength of neural responses recorded at all electrodes above all over the brain (Murray et  
178 al., 2008). The above formula was used to calculate the GFP for each time point from the

179 grand average data. For each ISI, grand averages were calculated by averaging epicranially-  
180 recorded auditory evoked potentials (eAEPs) of all animals. To represent the distribution of  
181 the surface potentials, we constructed topographic maps by interpolating voltage values  
182 between electrodes using Delaunay triangulation as described previously (Megevand et al.,  
183 2008). Note that this interpolation is for representation and the clustering algorithm was  
184 applied on raw EEG. Topographical mapping is a reference-free measure (Geselowitz, 1998)  
185 that represents global configuration of the underlying neuronal activity. Furthermore, it has  
186 been shown that different topographies are necessarily generated by different populations of  
187 neurons (Vaughan, 1982; Srebro, 1996). To take advantage of these topographies even more  
188 efficiently, rather than constructing topographies of a fixed time windows, we used a two-step  
189 clustering analysis. First, we used a topographic hierarchical clustering algorithm (Brunet et  
190 al., 2011) to identify the most dominant topographic maps in the grand averages of eAEPs  
191 representing the distribution of field potentials on the surface. For each ISI, a 500 ms epoch  
192 starting from the onset of the first tone was used for the clustering analysis. In our analysis,  
193 we restricted the number of clusters to a maximum of 20 while we did not impose a minimum  
194 threshold such that it was allowed to lead to a single cluster. Each cluster had to include at  
195 least four consecutive time points (4 ms). This analysis clusters multivariate signals into a  
196 sequence of potential maps based on the spatiotemporal similarity of voltage values across  
197 time while preserving maximum variance present in the data. Each cluster map (topographic  
198 map) is thought to represent a particular configuration of active generators within the brain  
199 during which the voltage potentials on the surface are stable. This constellation of active brain  
200 networks is reflected in a particular brain surface topography and is defined as a brain state.  
201 Subsequently, we fitted the result of clustering back to the grand average of the response  
202 following the second tone (T2) and to the time series of each mouse to statistically verify the  
203 first step of analysis and to test whether the cluster maps are shared among individual mice.

204 This step yields measures of presence, duration and power for each cluster map that can be  
205 statistically compared between different conditions.

206

### 207 Intracranial data analysis

208 Prior to any analysis, intracranially recorded data were low-pass filtered at 300 Hz and down-  
209 sampled to 1 KHz. The low-pass filtered signal contains local field potentials (LFPs) from  
210 which iAEPs were drawn. iAEPs were obtained by averaging across trials and grand averages  
211 were obtained by averaging across iAEPs of individual recordings. Latencies of iAEPs were  
212 calculated using the onset of the initial positive peak of the ICc and the onset of the main  
213 negative deflection of the Au1. For the ACC, the timestamp of the initial trough was  
214 considered as the latency. We used CSD as a guide to the best electrode channel in each  
215 recording session. Current source density (CSD) was estimated as the second spatial  
216 derivative of the LFP along the depth as described earlier (Megevand et al., 2008) according  
217 to the following formula:

$$CSD = \frac{V_{h-\Delta h} - 2 \cdot V_h + V_{h+\Delta h}}{\Delta h^2}$$

218 where  $V$  is the potential at position  $h$  and  $\Delta h$  is the distance between electrodes. CSD  
219 represents the spatiotemporal profile of extracellular current sinks and sources. To extract  
220 spectral characteristics of the LFPs, the signal was epoched containing segments that start 3  
221 before and end 3 s after each trial. To decompose the epoched LFP traces for frequency  
222 analysis, a family of complex morlet wavelets ( $\omega$ ) were used based on the following formula:

$$\omega_f = e^{i2\pi t f} e^{-t^2/(2\sigma^2)}$$

223 in which,  $i$  is the imaginary operator,  $t$  is time,  $f$  is frequency and  $\sigma$  represents the width of the  
224 wavelet.  $\sigma$ , the width of the wavelet, was defined as  $\lambda/(2\pi f)$  where  $\lambda$  is the number of wavelet  
225 cycles ranging from 4 to 10 (logarithmically spaced). The variable number of cycles was used

226 to account for the trade-off between temporal and frequency resolution of the analysis.  
227 Example single units presented in this study were extracted by automatic spike detection and  
228 clustering using Klusta (Rossant et al., 2016) followed by manual sorting.

229

### 230 **Statistical analysis**

231 Statistical analyses were performed using Matlab and Prism software (GraphPad). All  
232 statistics that are presented in this study concern group-level statistics based on the averaged  
233 data (e.g. AEP, power etc) of individual animals or recording sessions. Paired t-tests with  
234 Bonferroni corrections for multiple comparisons whenever applicable and one-way and two-  
235 way repeated measures ANOVAs followed by Tukey's post-hoc tests were used for  
236 comparisons among different conditions. For clustering analysis, the grand averaged data was  
237 first clustered followed by back-fitting to individual subjects. The results of fitting were then  
238 statistically tested using two-way ANOVAs. FDR corrected paired t-tests were used to  
239 determine a significant difference between GFP at individual timestamps compared to  
240 baseline GFP. Pearson correlation coefficients were calculated as a measure of signal  
241 similarity between different conditions. The specific contrasts and the statistical tests that  
242 have been employed to examine these contrasts are described wherever applicable.

243

244 **Results**

245 **Large-scale mapping of auditory evoked potentials in awake mice**

246 We first recorded auditory evoked potentials (AEPs) in awake animals using epicranial  
247 electrodes (eAEP) covering the entire dorsal surface of the brain (Fig. 1A). By considering the  
248 electric potential map at the surface of the brain, this method allows spatiotemporal analyses  
249 of the propagation of evoked activities at the large-scale level (Megevand et al., 2008). As  
250 illustrated in Figure 1B, a single tone (wideband noise) evokes large voltage waveforms  
251 (eAEP) invading all electrodes above the brain. Voltage topographies at the peaks of the  
252 global field power (GFP) curve shows that the activity is first dominated by a high amplitude  
253 positivity in the caudal region of the brain and later by high amplitude positivity in the lateral  
254 brain regions (Fig. 1B). These two regions of focal activity were localized at coordinates close  
255 to the inferior colliculus and the auditory cortices, respectively, which was confirmed by  
256 applying a source localization algorithm of the putative generators (Fig. 1C).

257 Although voltage topographies at individual time points could give insight into dominant  
258 brain processes at each time point, these processes often remain active for a period that  
259 encompasses several time points. In order to characterize the sequence of the large-scale brain  
260 processes following the auditory stimulation in more details, we clustered (Figure 1D) the  
261 surface maps of the grand average eAEPs ( $n = 7$  mice; first 120 ms) using a topographic  
262 hierarchical clustering algorithm (Megevand et al., 2008; Brunet et al., 2011). The optimal  
263 number of clusters to describe the grand mean data was determined by integrating a number  
264 of clustering measures such as global explained variance, cross-validation and Krzanovski-Lai  
265 criteria (Brunet et al., 2011). Since different map configuration represent different underlying  
266 neuronal generators, the cluster analysis allows to determine the different brain processes  
267 activated by the stimulus. By fitting these cluster maps back to the data (using spatial

268 correlation calculation and winner-takes-all labelling), the time period during which each of  
269 these maps are present can be determined (see Michel et al., 2001 for a detailed description of  
270 the method). Importantly, this fitting procedure results in a segmentation of the evoked  
271 potentials into time periods within which a certain scalp topography remains stable, indicating  
272 a particular brain state during information processing. The reproducibility of the clustering  
273 and fitting procedures was validated by back-fitting of the clusters to individual animals  
274 ERPs. Each map was present in at least 6 out of 7 animals and the sequential maps showed  
275 monotonically increasing onsets from map one to six. The differences of onsets and best  
276 correlation latencies between pairs of successive maps were all significant ( $p < 0.01$  for all).  
277 As shown in Figure 1D, the first stable map lasted 17 ms and was dominated by a large caudal  
278 activity presumably corresponding to the first station of the ascending auditory pathway that  
279 can be detected on the dorsal surface of the brain, i.e. the IC as explained above. During maps  
280 2 and 3 (between 18-25 and 25-54 ms post-T1, respectively), positive voltages become more  
281 lateral, surrounding a large area of relatively more negative potentials. This voltage  
282 configuration presumably reflects the curved lateral dipole orientations of the auditory cortical  
283 areas. Finally, maps 4 to 6 (between 55-80, 81-99 and 100-120 ms post-T1, respectively)  
284 show centro-frontal negativities that suggest a propagation of activity to the frontal regions  
285 (note that a significant focal brain activity can be reflected as local maxima or minima in  
286 voltage topographies). Therefore, this sequence of maps shows brain activities that likely  
287 correspond to main areas within the auditory pathway (i.e. inferior colliculus and auditory  
288 cortices) as well as higher order processing areas of prefrontal/anterior cingulate areas. Figure  
289 1E shows the intracranial recording sites and ERPs of an example subject. As expected, the  
290 onset of the evoked potentials recorded in the inferior colliculus correspond to the onset of the  
291 surface potentials recorded in the caudal region of the EEG. Intracranial recordings also  
292 confirm that auditory stimulation induced significant activities in the frontal cortical region.

293 **Long-lasting sensory gating of EEG-recorded auditory evoked potentials**

294 We then recorded surface EEG while paired auditory stimuli (wideband noise) were  
295 presented. The ISIs were randomly varied (125 – 2000 ms) across trials. As illustrated in EEG  
296 traces of an example subject in Figure 2, the eAEP and GFP amplitudes in response to the  
297 second tone are smaller as compared to the response to the first tone for all ISIs. This gating  
298 effect decreased with the duration of the ISI but was still present even at the longest ISI of 2  
299 sec. To quantify the effect of the duration of ISIs on the magnitude of sensory gating, we  
300 calculated the ratio of the peak-to-peak response magnitude of the second tone to that of the  
301 first tone at electrodes above the left and right auditory cortices (Fig. 2, left inset). A one-way  
302 repeated-measures ANOVA and post-hoc Tukey tests for multiple comparisons showed that  
303 the ratios were significantly lower than control ( $F(5, 30) = 103.2; p < 0.0001$ ) at all ISIs  
304 although the degree of gating was decreasing (i.e. bigger ratios) with increased ISIs. The ratio  
305 of the T1 responses of two randomly selected ISIs was used as control (minimum inter-trial  
306 intervals between two paired tones=8 sec). Note that T2 was still processed even at the  
307 shortest ISI (125) where the gating was the strongest, as it is visible from the small trough to  
308 peak component after T2 (see Fig. 2, top inset). This was confirmed by a one-sample t-test  
309 showing that the T2 response amplitudes were significantly larger than zero ( $t_6 = 4.62, p <$   
310  $0.01$ ).

311

312 **Decreased amplitude but unaltered topography of T2-evoked brain states for long**  
313 **ISIs**

314 Although classic method of measuring ASG gives information on the magnitude of gating, it  
315 neglects dynamics of simultaneous brain activity in other brain regions. Therefore, in order to  
316 examine the effects of sensory gating on large-scale brain networks, we used the clustering

317 analysis of the surface auditory evoked voltage maps described above. For this analysis, we  
318 first took epochs of 500 ms starting from T1 of the grand averages of the responses to T1 of  
319 all ISIs together. Figure 3A shows the result of this clustering (left panel) and the fitting of the  
320 resulting clusters on the grand average responses to T2 (right panel, 500 ms window from  
321 T2). The clustering of T1 grand average maps revealed a sequence of brain states similar to  
322 the one shown in Figure 1, indicating the propagation of activation across the auditory  
323 brainstem, the auditory cortex and the frontal brain regions. This sequence of brain states and  
324 its reproducibility was confirmed by back-fitting the clusters to the time series of individual  
325 animals: clustered maps were strongly stable across ISIs, as illustrated by the presence,  
326 correlation and max GFP parameters (Fig. 3C, red histograms and traces), even in the  
327 presence of T2 for the shortest ISIs (125 and 250 ms, see below). The stability of the brain  
328 states faded after approximately 350 ms post-T1 as no stable clusters were detected further on.  
329 This analysis suggests long lasting duration of stable brain states beyond initial AEP  
330 components determined in EEG or LFP traces. After this period (~350 ms), the strength of  
331 overall neural response was reduced to the baseline level as illustrated by the GFP values that  
332 were not significantly stronger than baseline (-200 to 0 ms; Fig. 3B).

333 For the ISI of 500 ms and longer, fitting these clustered maps evoked by T1 to the grand  
334 average eAEPs evoked by T2 indicated a similar sequence of topographies (Fig. 3) though  
335 with a reduced power, illustrating the effect of sensory gating. Thus, for ISIs of 500 ms and  
336 longer, decreasing the amplitude of the responses did not alter the sequence of voltage  
337 topographies, i.e. the spatial organization of the evoked brain states.

338

339

340

341 **Resistance of T1-evoked brain states at short ISIs**

342 Importantly, the clustering and fitting analyses revealed an important characteristic of the  
343 brain states: the sequence of brain states were not perturbed by T2 stimulations of short ISIs  
344 (125 and 250 ms) that take place within the post-T1 period of the evoked brain states. As  
345 shown in Figure 3A (left panel), the brain states of short ISIs at the time of T2 stimulation are  
346 similar to time-matched post-T1 brain states of long ISIs during which there is no T2 stimulus  
347 yet. This was confirmed by the fitting of the clustered maps onto the grand average eAEPs at  
348 125 and 250ms (Fig. 3A, right panel) and by the back-fitting to the time series of individual  
349 animals (Fig. 3C, blue histograms and traces) that revealed the absence of the earliest maps  
350 but the presence of maps 5-7 for T2 of the short ISIs. The continuity of brain states regardless  
351 of T2 stimulation following short ISIs was also confirmed by a model free comparison of  
352 voltage topographies of a fixed period immediately preceding or following T2 without using  
353 any clustering analysis (Fig. 4). As shown in this figure, the difference between pre-T2 and  
354 post-T2 GFPs is also approximately zero for the short ISIs suggesting lack of change in the  
355 power of the ongoing brain activity. Thus, the brain networks that are active at the moment of  
356 T2 stimulus continue to stay active despite T2 stimulation. These results suggest that the  
357 dominant generators of the brain states are resistant to perturbation by the new stimulus at the  
358 short ISIs and that the AEP induced dipoles are shadowed by still robust post-T1 dipoles  
359 generating those brain states. Thus, these analyses not only show long lasting stability of brain  
360 states beyond initial AEP components, but also suggest that these states are resistant against  
361 perturbation by T2.

362

363

364

### 365 Hierarchical enhancement of sensory gating

366 We then conducted intracranial recordings in ICc, Au1 or ACC (Fig. 5) to investigate local  
367 dynamics of brain processes with a greater precision. As expected, mean latencies of  
368 responses increase from the ICc region (n=12; 6.43±0.20 ms) to the Au1 (n=11; 10.71±0.24  
369 ms) and the ACC cortices (n=10; 15.69±0.24 ms). Figures 5A-C show example subjects'  
370 intracranially-recorded AEPs (iAEP; left panels) and peristimulus time histograms (PSTHs;  
371 right panels) in all three regions with a 500 ms ISI, illustrating the gating of T2 responses at  
372 the level of both iAEPs and single-unit firing. We computed the amplitude of iAEPs in all  
373 animals by measuring peak to peak magnitude of early iAEP components evoked by T1 and  
374 T2, as indicated in Figure 5 A-C. Repeated-measures two-way ANOVAs on the amplitude of  
375 iAEP components (Fig. 5D-F) revealed significant main effects of both ISI duration (F (4, 44)  
376 = 14.51;  $p < 10^{-4}$  & F (4, 40) = 16.84;  $p < 10^{-4}$  & F (5, 45) = 41.43;  $p < 10^{-4}$  for the ICc, Au1  
377 and ACC respectively) and tone (T1 or T2; F (1, 11) = 32.29;  $p < 10^{-4}$  & F (1, 10) = 18.84;  $p$   
378 < 0.002 & F (1, 9) = 86.14;  $p < 10^{-4}$  for the ICc, Au1 and ACC respectively) and a significant  
379 tone x ISI interaction ( $p < 10^{-4}$ ). Bonferroni post-hoc tests corrected for multiple comparisons  
380 revealed a significant decrease ( $p < 0.001$ ) in the amplitude of T2 response at all ISIs except  
381 2000 ms in the ICc and Au1 and 1000 ms in the Au1. In the ACC, there was a significant  
382 reduction at all ISIs including 2000 ms ( $p < 0.05$  for 2000 ms and  $p < 0.001$  for all other ISIs).  
383 The area between the T1 and T2 response curves is an indication of the magnitude of sensory  
384 gating (Fig. 5D-F); the two curves converge as the ISI increases, because of the reduction of  
385 gating at longer ISIs. We further quantified sensory gating at each region by dividing the  
386 amplitude of iAEP components of T2 to those of T1 (Figure 5G). The first negative peaks in  
387 the ICc and Au1 were significantly gated at all ISIs but 2000 ( $p < 0.001$  for the ISIs of 125,  
388 250 and 500 and  $p < 0.05$  for the ISI of 1000). In the ACC, the ratios were significantly  
389 different from the control at all ISIs ( $p < 0.05$  for the ISI of 2000 and  $p < 0.001$  for all other

390 ISIs). Note that confirming surface EEG results, intracranial recordings also showed that the  
391 T2 is indeed processed even at the shortest ISI despite being strongly gated. This was  
392 statistically confirmed by one-sample t-tests of ASG ratios for the shortest ISI that revealed  
393 significantly larger ratios than zero at all three regions ( $p < 0.001$  for the ICc and Au1,  $p <$   
394  $0.05$  for the ACC). This confirms that the T2 was indeed processed across the hierarchy  
395 despite being strongly gated. In addition to the decreased magnitude of gating with increasing  
396 ISIs, the average T2/T1 ratios (Fig. 5G) illustrates another important aspect of sensory gating  
397 across different brain regions: the magnitude of gating progressively increases as we go from  
398 the auditory brainstem to the primary auditory cortex (Au1) and anterior cingulate cortex  
399 (ACC) suggesting a hierarchical enhancement of sensory gating. Two-way ANOVA (ISI  
400 duration and brain regions (ICc, Au1 and ACC) as factors) on the gating (T2/T1 ratios) with  
401 repeated measures on one factor (ISI duration) showed a main effect of the brain region ( $F(2,$   
402  $30) = 40.92; p < 10^{-4}$ ) statistically corroborating the hierarchical enhancement of the ASG.

403

#### 404 **Effects of the second tone on the LFP at the shortest ISI**

405 While local networks process T2 stimulus, the brain states remain unaltered for a period that  
406 encompasses short ISIs. Epicranial EEG revealed that the evoked brain states were resistant to  
407 perturbation by the new stimulus at the shortest ISIs, i.e when T2 arrives during the evoked  
408 brain states. How this stability and resistance (against perturbation) of the brain states are  
409 reflected in the activity of local networks in the auditory pathway (ICc and Au1) and ACC?  
410 Might there be traces of stability in these signals even though T2 stimulus is processed? We  
411 therefore further examined the similarity between short-ISI post-T2 iAEPs with time-matched  
412 long-ISI iAEPs. We calculated linear dependence between these signals using Pearson  
413 correlation coefficient. Coefficient of zero corresponds to absolutely inconsistent signals  
414 whereas coefficient of 1 corresponds to identical signals. Note that this measure takes into

415 account signal trajectory across time and ignores scaling in the magnitude of the signal.  
416 Morphologically coherent signals across time will be highly correlated even if the amplitudes  
417 are markedly different. Therefore, this is an ideal measure to address whether T2 stimulation  
418 at different time points abolishes signal similarity or a degree of similarity survives despite T2  
419 stimulation. Figures 6A-C show visual similarity of iAEPs during the 350 ms window after  
420 T1 between a short ISI (125 ms) and a long ISI (1000 ms) conditions, i.e. with or without T2,  
421 of example recordings in the ICc, Au1 and ACC, respectively. Analysis of correlation  
422 coefficients between post-T2 epochs of short ISIs with the time-matched period of post-T1  
423 epochs of long ISIs revealed a significantly higher similarity than pre-T1 baseline epochs for  
424 the ISI of 125ms ( $p < 0.001$ ,  $p < 0.05$  and  $p < 0.01$  for the ICc, Au1 and ACC respectively)  
425 supporting the extended brain stability suggested by the clustering analysis of the scalp EEG.  
426 There was a non-significant trend for the ISI of 250 ms but there was no correlation for the  
427 ISI of 500 ms (Fig. 6D-E).

428

#### 429 **Does pre-T2 activities can predict sensory gating?**

430 Sensory gating is long-lasting and the second stimulus is attenuated even after 2000 ms which  
431 is far beyond the remaining processes following T1 stimulation which lasts approximately up  
432 to 350 ms post-T1 (Fig. 3B). The brain states just before T2 may predict the ASG and  
433 therefore, pre-T2 signals in epicranial and intracranial recordings have to be studied in order  
434 to evaluate the role of pre-state dynamics on the ASG. As shown in Figure 4, the pre-T2  
435 states, calculated from the epicranial EEG recordings, are different across different ISIs.  
436 Global field power of these states are significantly different from baseline at short ISIs but not  
437 for ISIs of 500 ms and longer. These results indicate that the brain states we observed just  
438 before T2 does not explain the ASG. The iAEPs and power (induced) spectra of pre-T2  
439 intracranially recorded LFPs are also depicted in Figure 7. As shown in this Figure (left

440 panels), it takes close to 500 ms for the iAEPs to reach steady state baseline levels. This is  
441 consistent with the previous analysis on the similarity of LFPs (Fig. 6) where we showed a  
442 significant similarity between post-T2 LFPs of short ISIs and time-matched post-T1 LFPs of  
443 long ISIs indicating that the traces of the response to T1 could be found after T2 when the ISI  
444 is short. Subsequently, we calculated power spectra of a long ISI condition (2000 ms) during  
445 baseline and during 125ms segments prior to time matching T2 of 250 and 500ms ISIs  
446 (highlighted periods) (Fig. 7; right panels) in order to avoid T2 response spectral leakage. The  
447 results of this analysis were consistent with the GFP computed from the epicranial recordings  
448 (Fig. 3B) and showed that the pre-T2 induced power was different from the baseline for 250  
449 ms ISI but not for 500 ms ISI. Note that the power is significantly higher than the baseline up  
450 to 500 ms in the ICc. Taken together, we did not identify ongoing activity just before T2 for  
451 long ISIs that is significantly different from the baseline that could explain the gating of the  
452 imminent T2 response.

453

#### 454 **Auditory sensory gating in ventral cochlear nucleus**

455 Despite the controversy about the origins of ASG, we showed that the ASG exists at the level  
456 of the ICc consistent with the indirect evidence (Malmierca et al., 2009) suggesting sensory  
457 specific adaptation at the ICc. Given this controversy and the lack of common understanding  
458 of the mechanisms of ASG, we recorded the activity of neurons at the entry of the auditory  
459 stimuli in the CNS in the ventral cochlear nucleus (vCN). The analysis of these recordings  
460 showed that indeed ASG already exists at the first station of auditory pathway in the CNS  
461 (Fig. 8). Note that the degree of gating in the vCN is similar to that of the ICc but we do not  
462 directly compare the gating in the vCN to other regions in the hierarchy since these recordings

463 are based on fewer number of animals and we suggest a more comprehensive study of the role  
464 of vCN in the ASG.

465 **Discussion**

466 We used variable inter-stimulus intervals (ISIs) and both epicranial and intracranial  
467 recordings to investigate large-scale brain networks governing auditory sensory gating (ASG).  
468 We demonstrate that the ASG is long-lasting, takes place in areas ranging as early as the vCN  
469 and ICc to higher order areas of Au1 and ACC and is hierarchically organized. Furthermore,  
470 we show that auditory stimulation results in the activation of a sequence of stable brain  
471 networks lasting up to approximately 350 ms. During this period, the second tone (i.e. ISIs of  
472 125 and 250 ms) of paired stimuli does not change the architecture of brain topographies  
473 evoked by the first tone suggesting that induced networks resist perturbation by incoming  
474 stimuli. This was evidenced by a striking similarity between voltage topographies  
475 representing active brain networks following T2 in short duration ISIs (i.e. 125 and 250 ms)  
476 and time-matched post-T1 topographies in long duration ISIs (i.e. 500, 1000 and 2000 ms) as  
477 well as a corresponding similarity between intracranially recorded LFPs. After this period, the  
478 brain reaches a baseline activity level and a second auditory stimulus induces similar network  
479 as the first stimulus. However, gating is preserved at least up to 2000 ms at the level of the  
480 amplitude of the neural responses.

481 Given the clinical relevance of ASG in which the degree of gating of the T2 is used as a  
482 pathological biomarker of schizophrenia (Javitt and Sweet, 2015), most studies concerning  
483 ASG has used the same ISI as in the clinics, i.e. 500 ms (Kurthen et al., 2007; Rihs et al.,  
484 2013; Oranje and Glenthøj, 2014). At different timescales ranging from tens of milliseconds  
485 to a couple of seconds, distinct brain mechanisms might be responsible for gating of the  
486 response to T2 (Ulanovsky et al., 2004; Wehr and Zador, 2005). Our approach using variable  
487 ISIs in conjunction with epicranial and intracranial recordings enabled us to characterize ASG  
488 at global brain networks level and selected individual brain regions across a range of  
489 timescales. Although a few studies have used different ISI durations to study ASG (Wehr and

490 Zador, 2005; Mears et al., 2006), these studies have usually been limited to one or two brain  
491 areas and not systematically characterized the effects of ISI duration on ASG. Our  
492 experiments revealed three characteristics of the ASG: first, there was still significant gating  
493 after an ISI of 2000 ms (longest in our experiments). Note that there was no detectable  
494 activity remaining from the T1 processing at long ISIs, and the GFP and local brain activity  
495 were similar to the baseline at ISIs of 500 ms or longer. Second, regardless of the mechanisms  
496 involved, there was a monotonically decreasing magnitude of ASG as the ISI increases (Figs.  
497 2 and 5). This suggests that either the mechanisms involved in the ASG at short intervals (e.g.  
498 synaptic inhibition) are stronger than those involved in longer ISIs or the mechanisms that act  
499 at longer ISIs are also active at short intervals and therefore there is a synergy between  
500 mechanisms acting at short intervals. Multiple local, bottom-up and/or top-down mechanisms  
501 may be responsible for ASG and deciphering their relative contributions needs further  
502 research. Based on our data, however, we can suggest (i) the fact that pre-T2 states were  
503 different across different ISIs and (ii) could not predict whether the arriving T2 will be gated  
504 or not and (iii) the fact that the T1-induced activity regresses back to the baseline level before  
505 500 ms indicates that these mechanisms act earlier but their effects (e.g. synaptic depression)  
506 are long-lasting. Third, the dynamics of gating in the ICc, Au1 and ACC suggests a  
507 progressively amplified ASG across the hierarchy. Using ISIs ranging from 64 to 512 ms,  
508 Wehr and Zador (2005) suggested that it is unlikely that ASG in auditory cortical neurons at  
509 ISIs longer than 100 ms is inherited from earlier auditory brain areas and proposed that  
510 intracortical or thalamocortical synaptic depression is the likely mechanism of sensory gating  
511 at these intervals. In our experiments, the existence of strong gating at long ISIs in areas as  
512 early as vCN and ICc in the auditory pathway suggest that gating of cortical neurons is partly  
513 inherited from earlier brain regions. Although SSA has been demonstrated in the non-  
514 lemniscal regions of subcortical inferior colliculus (Malmierca et al., 2009), ASG at the level

515 of inferior colliculus has not been clearly addressed. Our results demonstrate that indeed  
516 sensory gating takes place in the inferior colliculus centralis. This is consistent with studies on  
517 sensory specific adaptation (SSA) which also suggest a degree of adaptation in subcortical  
518 brain regions such as the ICc (Malmierca et al., 2009) and auditory thalamus (Antunes et al.,  
519 2010). Furthermore, unlike previous studies suggesting lack of SSA in vCN (Ayala et al.,  
520 2012), we showed significant ASG even at the level of vCN, which is the first auditory  
521 processing station in the CNS. While ASG and SSA are related phenomena in the auditory  
522 processing, there are differences in the paradigms used to study these two phenomena.  
523 Therefore, it is very likely that the discrepancy between our results and those of Ayala and  
524 colleagues emanates from the differences in the employed paradigms and indicates distinct  
525 characteristics of neural processing of auditory information. Our results showing sensory  
526 gating at the first station of auditory processing in the CNS enhance the plausibility of the  
527 hypothesis that the sensory gating is a basic property of the brain hardwired in brain network  
528 assemblies, without ruling out the possibility that subcortical ASG maybe be driven by top-  
529 down cortical projections to the brainstem. On the other hand, the fact that we demonstrate a  
530 progressively amplified sensory gating across hierarchy, suggests that further thalamocortical  
531 and cortical mechanisms such as synaptic depression and feedback regulation enhance the  
532 magnitude of gating in Au1 and particularly ACC. This suggests a link between higher  
533 cognitive brain areas and low-level sensory processing and highlights the translational  
534 importance of low-level sensory processing mechanisms for disorders of higher cognitive  
535 functions as proposed by Javitt and Sweet (2015).

536 What is the state of brain networks following auditory sensory stimulation? In other words,  
537 how the dipoles across brain regions are configured following the stimulus? The stability of  
538 brain states activated by the T1 suggests that the dynamics of the activity of all dipoles result  
539 in a reproducible sequence of brain states during which distinct subsets of those dipoles are

540 simultaneously active. Topographic mapping is a reference-free measure that represents  
541 global configuration of the underlying neuronal activity (Geselowitz, 1998) and based on the  
542 laws of physics, changes in voltage topographies reflect changes in underlying generators  
543 (Vaughan, 1982). The clustering method that we used (Megevand et al., 2008; Brunet et al.,  
544 2011) divides the potential maps into meaningful clusters during which there is no change in  
545 topographic maps. Each cluster represents a particular brain state and is generated by a  
546 network of roughly simultaneously active sources (Michel and Koenig, 2018). Importantly,  
547 the stability of brain states extend far beyond the initial evoked potentials and lasts as long as  
548 350 ms even in the absence of a goal-directed behavior associated with the tone as was the  
549 case in our experiments. Thus, we suggest that brain dwells back in the baseline resting state  
550 after this sequence of activated brain states fades. Finally, the stability and reproducibility of  
551 the configuration of all brain dipoles was robust such that a second identical tone, presented  
552 during this period, was unable to bring about a change in the architecture of sequential brain  
553 states ensuing T1 (Fig. 3). Note that this resistance of brain states to perturbation by T2 is not  
554 due to the fact that T2 is not processed (Fig. 2 & 5). Consistent with this brain network  
555 stability notion, a recent fMRI study among human participants showed that indeed brain  
556 networks are stable at individual participants' level and task states only modestly influences  
557 brain networks (Gratton et al., 2018). Investigating local brain activity using intracranial  
558 recordings provides further support for the results discussed above. First, it demonstrates that  
559 T2 has been processed across the hierarchy (Figs. 5 and 6A-C) despite being strongly gated.  
560 Second, it supports the global brain network stability by showing traces of similarity between  
561 post-T2 LFPs of short ISIs and LFPs of time-matched long ISIs. Linear dependence of these  
562 LFP segments suggest that indeed there is a significant similarity in the morphology of signals  
563 between post-T2 period of the shortest ISI and time-matched period of long ISIs. This  
564 supports the resistance of the brain states to perturbation at short intervals by showing

565 common features in the brain signal (oscillatory or non-oscillatory) regardless of T2  
566 stimulation at short intervals. We suggest it is possible that membrane potentials of  
567 subpopulations of neurons continue to reverberate resulting in the long lasting and stable  
568 responses. However, the exact cellular mechanisms underlying the stability and resistance  
569 (against perturbation) of brain responses demand further investigation.

570 Might the extended brain stability represent a fundamental property of brain function? Might  
571 it have a functional role? Our experiments suggest that the extended stability of brain states  
572 and their resistance against perturbation may result from two factors: The strength of global  
573 brain networks as evidenced by the GFP (Fig. 3B) and the strong sensory gating of T2  
574 response during this period (Figs. 2 and 5). These two factors are interdependent and both  
575 may contribute to the resistance of stable brain states against perturbation at short ISIs. Future  
576 studies should examine whether there is a causal relationship between these two. Extended  
577 brain stability may also represent a way for the brain to integrate the stimulus with other  
578 information available from internal and external sources and further interpret the stimulus  
579 significance after an initial and fast processing of the sound itself. Finally, it may involve  
580 attentional activation of brain regions to prepare for an upcoming event or to inhibit activated  
581 brain regions in case of discarding the stimulus.

582

583 **References:**

- 584 Adler LE, Pachtman E, Franks RD, Pecevich M, Waldo MC, Freedman R (1982) Neurophysiological  
585 evidence for a defect in neuronal mechanisms involved in sensory gating in schizophrenia.  
586 *Biol Psychiatry* 17:639-654.
- 587 Alho K, Woods DL, Algazi A, Knight RT, Naatanen R (1994) Lesions of frontal cortex diminish the  
588 auditory mismatch negativity. *Electroencephalogr Clin Neurophysiol* 91:353-362.
- 589 Antunes FM, Nelken I, Covey E, Malmierca MS (2010) Stimulus-specific adaptation in the auditory  
590 thalamus of the anesthetized rat. *PLoS One* 5:e14071.
- 591 Ayala YA, Perez-Gonzalez D, Duque D, Nelken I, Malmierca MS (2012) Frequency discrimination and  
592 stimulus deviance in the inferior colliculus and cochlear nucleus. *Front Neural Circuits* 6:119.
- 593 Brosch M, Schreiner CE (1997) Time course of forward masking tuning curves in cat primary auditory  
594 cortex. *J Neurophysiol* 77:923-943.
- 595 Brunet D, Murray MM, Michel CM (2011) Spatiotemporal analysis of multichannel EEG: CARTOOL.  
596 *Comput Intell Neurosci* 2011:813870.
- 597 Christianson GB, Sahani M, Linden JF (2011) Depth-dependent temporal response properties in core  
598 auditory cortex. *J Neurosci* 31:12837-12848.
- 599 Cromwell HC, Anstrom K, Azarov A, Woodward DJ (2005) Auditory inhibitory gating in the amygdala:  
600 single-unit analysis in the behaving rat. *Brain Res* 1043:12-23.
- 601 Duque D, Malmierca MS, Caspary DM (2014) Modulation of stimulus-specific adaptation by GABA(A)  
602 receptor activation or blockade in the medial geniculate body of the anaesthetized rat. *J*  
603 *Physiol* 592:729-743.
- 604 Friston K (2018) Does predictive coding have a future? *Nat Neurosci* 21:1019-1021.
- 605 Geselowitz DB (1998) The zero of potential. *IEEE Eng Med Biol Mag* 17:128-132.
- 606 Giraud AL, Arnal LH (2018) Hierarchical Predictive Information Is Channeled by Asymmetric  
607 Oscillatory Activity. *Neuron* 100:1022-1024.
- 608 Gratton C, Laumann TO, Nielsen AN, Greene DJ, Gordon EM, Gilmore AW, Nelson SM, Coalson RS,  
609 Snyder AZ, Schlaggar BL, Dosenbach NUF, Petersen SE (2018) Functional Brain Networks Are  
610 Dominated by Stable Group and Individual Factors, Not Cognitive or Daily Variation. *Neuron*  
611 98:439-452 e435.
- 612 Grunwald T, Boutros NN, Pezer N, von Oertzen J, Fernandez G, Schaller C, Elger CE (2003) Neuronal  
613 substrates of sensory gating within the human brain. *Biol Psychiatry* 53:511-519.
- 614 Javitt DC, Freedman R (2015) Sensory processing dysfunction in the personal experience and  
615 neuronal machinery of schizophrenia. *Am J Psychiatry* 172:17-31.
- 616 Javitt DC, Sweet RA (2015) Auditory dysfunction in schizophrenia: integrating clinical and basic  
617 features. *Nat Rev Neurosci* 16:535-550.
- 618 Knott V, Millar A, Fisher D (2009) Sensory gating and source analysis of the auditory P50 in low and  
619 high suppressors. *Neuroimage* 44:992-1000.
- 620 Kurthen M, Trautner P, Rosburg T, Grunwald T, Dietl T, Kuhn KU, Schaller C, Elger CE, Urbach H,  
621 Elisevich K, Boutros NN (2007) Towards a functional topography of sensory gating areas:  
622 invasive P50 recording and electrical stimulation mapping in epilepsy surgery candidates.  
623 *Psychiatry Res* 155:121-133.
- 624 Lehmann D, Skrandies W (1980) Reference-free identification of components of checkerboard-  
625 evoked multichannel potential fields. *Electroencephalogr Clin Neurophysiol* 48:609-621.
- 626 Malmierca MS, Cristaudo S, Perez-Gonzalez D, Covey E (2009) Stimulus-specific adaptation in the  
627 inferior colliculus of the anesthetized rat. *J Neurosci* 29:5483-5493.
- 628 Mayer AR, Hanlon FM, Franco AR, Teshiba TM, Thoma RJ, Clark VP, Canive JM (2009) The neural  
629 networks underlying auditory sensory gating. *Neuroimage* 44:182-189.
- 630 Mears RP, Klein AC, Cromwell HC (2006) Auditory inhibitory gating in medial prefrontal cortex: Single  
631 unit and local field potential analysis. *Neuroscience* 141:47-65.

- 632 Megevand P, Quairiaux C, Lascano AM, Kiss JZ, Michel CM (2008) A mouse model for studying large-  
633 scale neuronal networks using EEG mapping techniques. *Neuroimage* 42:591-602.
- 634 Michel CM, Koenig T (2018) EEG microstates as a tool for studying the temporal dynamics of whole-  
635 brain neuronal networks: A review. *Neuroimage* 180:577-593.
- 636 Michel CM, Thut G, Morand S, Khateb A, Pegna AJ, Grave de Peralta R, Gonzalez S, Seeck M, Landis T  
637 (2001) Electric source imaging of human brain functions. *Brain Res Brain Res Rev* 36:108-118.
- 638 Murray MM, Brunet D, Michel CM (2008) Topographic ERP analyses: a step-by-step tutorial review.  
639 *Brain Topogr* 20:249-264.
- 640 Niven JE, Laughlin SB (2008) Energy limitation as a selective pressure on the evolution of sensory  
641 systems. *J Exp Biol* 211:1792-1804.
- 642 Oranje B, Glenthøj BY (2014) Clonidine normalizes levels of P50 gating in patients with schizophrenia  
643 on stable medication. *Schizophr Bull* 40:1022-1029.
- 644 Paxinos G, Franklin KBJ (2004) *The mouse brain in stereotaxic coordinates*, Compact 2nd Edition.  
645 Amsterdam ; Boston: Elsevier Academic Press.
- 646 Qi R, Li M, Ma Y, Chen N (2015) State-dependent changes in auditory sensory gating in different  
647 cortical areas in rats. *PLoS One* 10:e0126684.
- 648 Quairiaux C, Sizonenko SV, Megevand P, Michel CM, Kiss JZ (2010) Functional deficit and recovery of  
649 developing sensorimotor networks following neonatal hypoxic-ischemic injury in the rat.  
650 *Cereb Cortex* 20:2080-2091.
- 651 Rao RP, Ballard DH (1999) Predictive coding in the visual cortex: a functional interpretation of some  
652 extra-classical receptive-field effects. *Nat Neurosci* 2:79-87.
- 653 Rihs TA, Tomescu MI, Britz J, Rochas V, Custo A, Schneider M, Debbane M, Eliez S, Michel CM (2013)  
654 Altered auditory processing in frontal and left temporal cortex in 22q11.2 deletion syndrome:  
655 a group at high genetic risk for schizophrenia. *Psychiatry Res* 212:141-149.
- 656 Rossant C, Kadir SN, Goodman DFM, Schulman J, Hunter MLD, Saleem AB, Grosmark A, Belluscio M,  
657 Denfield GH, Ecker AS, Tolias AS, Solomon S, Buzsaki G, Carandini M, Harris KD (2016) Spike  
658 sorting for large, dense electrode arrays. *Nat Neurosci* 19:634-641.
- 659 Srebro R (1996) A bootstrap method to compare the shapes of two scalp fields. *Electroencephalogr*  
660 *Clin Neurophysiol* 100:25-32.
- 661 Ulanovsky N, Las L, Farkas D, Nelken I (2004) Multiple time scales of adaptation in auditory cortex  
662 neurons. *J Neurosci* 24:10440-10453.
- 663 Vaughan HG, Jr. (1982) The neural origins of human event-related potentials. *Ann N Y Acad Sci*  
664 388:125-138.
- 665 Wehr M, Zador AM (2005) Synaptic mechanisms of forward suppression in rat auditory cortex.  
666 *Neuron* 47:437-445.
- 667 Williams TJ, Nuechterlein KH, Subotnik KL, Yee CM (2011) Distinct neural generators of sensory gating  
668 in schizophrenia. *Psychophysiology* 48:470-478.
- 669 Witten L, Bastlund JF, Glenthøj BY, Bundgaard C, Steiniger-Brach B, Mork A, Oranje B (2016)  
670 Comparing Pharmacological Modulation of Sensory Gating in Healthy Humans and Rats: The  
671 Effects of Reboxetine and Haloperidol. *Neuropsychopharmacology* 41:638-645.
- 672 Yu YQ, Xiong Y, Chan YS, He J (2004) Corticofugal gating of auditory information in the thalamus: an  
673 in vivo intracellular recording study. *J Neurosci* 24:3060-3069.

674

675

676 **Figure Legends:**

677 **Figure 1:** Auditory evoked potential (AEP) in an example subject with epicranial recording.

678 **A)** Shows an awake head-fixed animal during epicranial recording (left) and corresponding  
679 electrode placement map on the surface of the skull. **B)** illustrates the eAEP of an example  
680 subject following auditory sensory stimulation. The lower trace (blue) depicts the GFP of the  
681 shown EEG traces (average of 32 trials). The traces are time-locked to auditory stimulation  
682 (red bar at time zero) and two gray lines correspond to two GFP peaks. Voltage topographic  
683 maps at two time points with a peak GFP are shown at the top. **C)** respective source localized  
684 maps of the two topographies shown in B suggesting localization of main generators in the  
685 inferior colliculus and auditory cortex. The upper map represents a sagittal section of ~0.6  
686 mm lateral to the midline. The axes of orientations for the 3D map is also provided. A, P, D,  
687 V, and L refer to anterior, posterior, dorsal, ventral and lateral orientations, respectively. **D)**  
688 Clustering (top) of the auditory response shows a sequence of topographies (bottom)  
689 corresponding to the large scale network processing auditory response. The temporal extent of  
690 the identified maps appears as segments of the grand average global field power trace. Back-  
691 fitting of the clusters to individual animals' ERPs validated the clustering analysis  
692 reproducibility across subjects as it showed monotonically increasing onsets and latencies of  
693 best correlation of each component map. Onset and latency differences between pairs of  
694 successive maps were all significant ( $p < 0.01$ ). **E)** Schematic representation of intracranial  
695 recording sites (top) and intracranial ERPs of example subjects recorded from the ICc, Au1  
696 and ACC.

697

698 **Figure 2:** Epicranial EEG recording of sensory gating using paired-tone paradigm.

699 The eAEP of an example subject (same as figure 1B) to a pair of tones with different ISIs are  
700 shown. The red traces correspond to left and right electrodes above the auditory cortex and  
701 black traces represent all other electrodes. The blue circles indicate the peak-to-peak  
702 amplitude used to quantify SG. Top inset shows the zoomed segment (only electrodes above  
703 auditory cortices) within the dashed rectangle to highlight the strongly gated but still present  
704 response to T2 at the ISI of 125 ms. The blue trace in bottom of each EEG trace corresponds  
705 to the GFP. The attenuation (gating) of the response to the second tone is visually clear. The  
706 left inset shows average sensory gating ratios ( $n = 7$  mice) quantified based on the eAEPs of  
707 auditory electrodes. Note that even at 2000 ms ISI, there is a significant sensory gating. The  
708 ratio equal to 1 means no gating and the smaller the ratios are, the stronger the gating is. Error  
709 bars indicate standard error of mean (SEM). \*  $p < 0.05$ ; \*\*\* $p < 0.001$ .

710

711 **Figure 3:** Similarity of functional brain states during post-T2 of short ISIs and time-matched  
712 period of long ISIs during which there is no T2 yet.

713 **A)** Left panel shows the result of the clustering analysis of the grand-average eAEP during the  
714 500 ms period following T1. During this period, T2 takes place in short-ISI conditions but not  
715 in the long ISIs. The corresponding spatiotemporal topographic maps are presented below.  
716 Each map is labeled with the same color code that is used for the clusters. The result of  
717 clustering was fitted on the post-T2 epochs (right panel) revealing that the same sequence of  
718 brain states was activated in response to the second tone after long ISIs as compared to the  
719 sequence following the first tone. For short ISIs, it shows that initial segments of T1 sequence  
720 were curtailed and suggests that the cluster sequences continue from where T2 stimulation  
721 enters in the timecourse. **B)** shows the GFP at a representative ISI (500 ms). The thick line  
722 indicates *fdr*-corrected significant enhancement of global field power compared to baseline (-  
723 200 to 0) power. **C)** displays the quantitative fitting results of the clusters across individual

724 subjects. “Presence” histograms show the number of the animals having a given topographic  
725 map. Note general similarity of presence, correlation and power of T1 (red) across different  
726 ISI conditions regardless of the presence or absence of T2 stimulation. This is also  
727 demonstrated by the convergence of correlation and power curves of T2 (blue) to those of T1  
728 after maps 5 and 6 for ISIs of 125 and 250, respectively.

729

730 **Figure 4:** Similarity of pre-T2 and post-T2 maps at short ISIs.

731 A) The topographic maps of of pre-T2 and post-T2 EEG (20 ms each) are shown separately  
732 for each ISI. At short ISIs, visually distinguishable similarities exist between pre-T2 and post-  
733 T2 maps. B) show pre-T2, post-T2 and and the difference between them across different ISIs.  
734 As shown on the left panel, pre-T2 GFPs are higher for ISIs of 125 and 250. There is also  
735 approximately zero change in power from pre-T2 to post-T2 at these ISIs.

736

737 **Figure 5:** Sensory gating in intracranial signals recorded from ICc, Au1 and ACC.

738 **A-C)** Example iAEPs (left panels) and PSTHs (of all units recorded during a single session)  
739 recorded from the ICc, Au1 and ACC, respectively. Magenta dots represent peak-to-peak  
740 measurement of the first major ERP component at each region. Latencies were calculated  
741 using the onsets of the initial positive peak for the ICc, the main negative deflection for the  
742 Au1, and the initial trough for the ACC. **D-F)** Amplitude of ERP components measured as  
743 indicated in (A-C) in each region (i.e., ICc (n = 12), Au1 (n = 11), and ACC (n = 10)) in  
744 response to the first (red) and second (blue) tones. The larger the area between two curves is,  
745 the stronger the SG is. **G)** The ratio of sensory gating for different components. The gating  
746 increases progressively from the ICc through auditory ERP to the ACC ERP. Error bars  
747 signify standard error of mean (SEM).

748

749 **Figure 6:** Similarity of post-T2 LFPs of short ISIs to time-matched LFPs of long ISIs.

750 **A, B, C)** Show iAEPs of example recordings during 125 (top panels) and 1000 ms (bottom  
751 panels) ISIs. Highlighted periods represent pre-T1 baseline and period of interest (125-250 ms  
752 post-T1). Dashed lines represent Z-scores corresponding to  $p$  values of 0.05. **D, E, F)**  
753 Correlation coefficient of LFP time series of post-T2 trials during ISIs of 125, 250 and 500 ms  
754 with time-matched (i.e. 125-250; 250-375; and 500-625 ms post-T1 respectively) period of  
755 1000 and 2000 ms ISIs. This coefficient is based on the convolution of the signals and takes  
756 into account the temporal dynamics of the signal. As it is seen in the figure, post-T2 time  
757 series at short ISIs were significantly correlated to the time-matched period in long ISIs  
758 compared to baseline correlations. This correlation deteriorates as the ISI duration increases  
759 such that there is a non-significant trend at 250 ms ISI and the correlation coefficient is not  
760 different than the baseline at 500 ms ISI.

761

762 **Figure 7:** Pre-state dynamics following T1 and prior to T2 auditory stimulation

763 **A-C)** Left panels show grand average ERPs across all recordings during ISIs of 250 (top  
764 panels) and 500 (bottom panels) for the ICc ( $n=12$ ), Au1 ( $n=11$ ) and ACC ( $n=10$ ),  
765 respectively. Right top panels show the corresponding grand average iAEPs calculated for the  
766 same time length relative to T1 as the left panels but without a second tone, i.e. based on the  
767 2000 ms long ISI. The gray shades around iAEPs indicate SEM. Bottom right panels show the  
768 induced power levels during segments corresponding to pre T2 periods for 250ms ISI (green  
769 highlighted segment in the iAEPs) and 500ms ISI (blue segment), as compared to the baseline  
770 (grey segment). The thick blue lines indicate  $fdr$ -corrected significant difference between  
771 power of these periods compared to that of the baseline period.

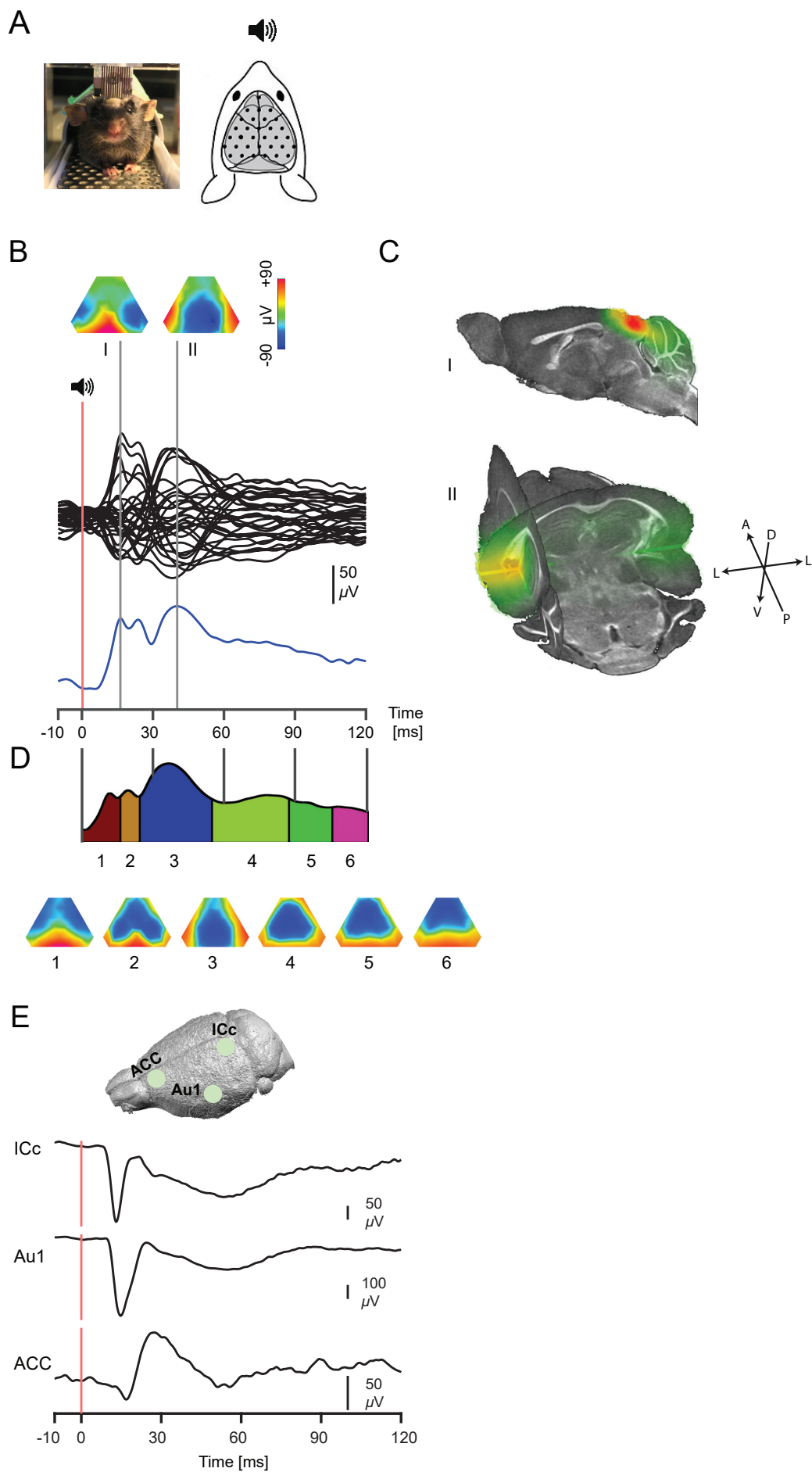
772

773

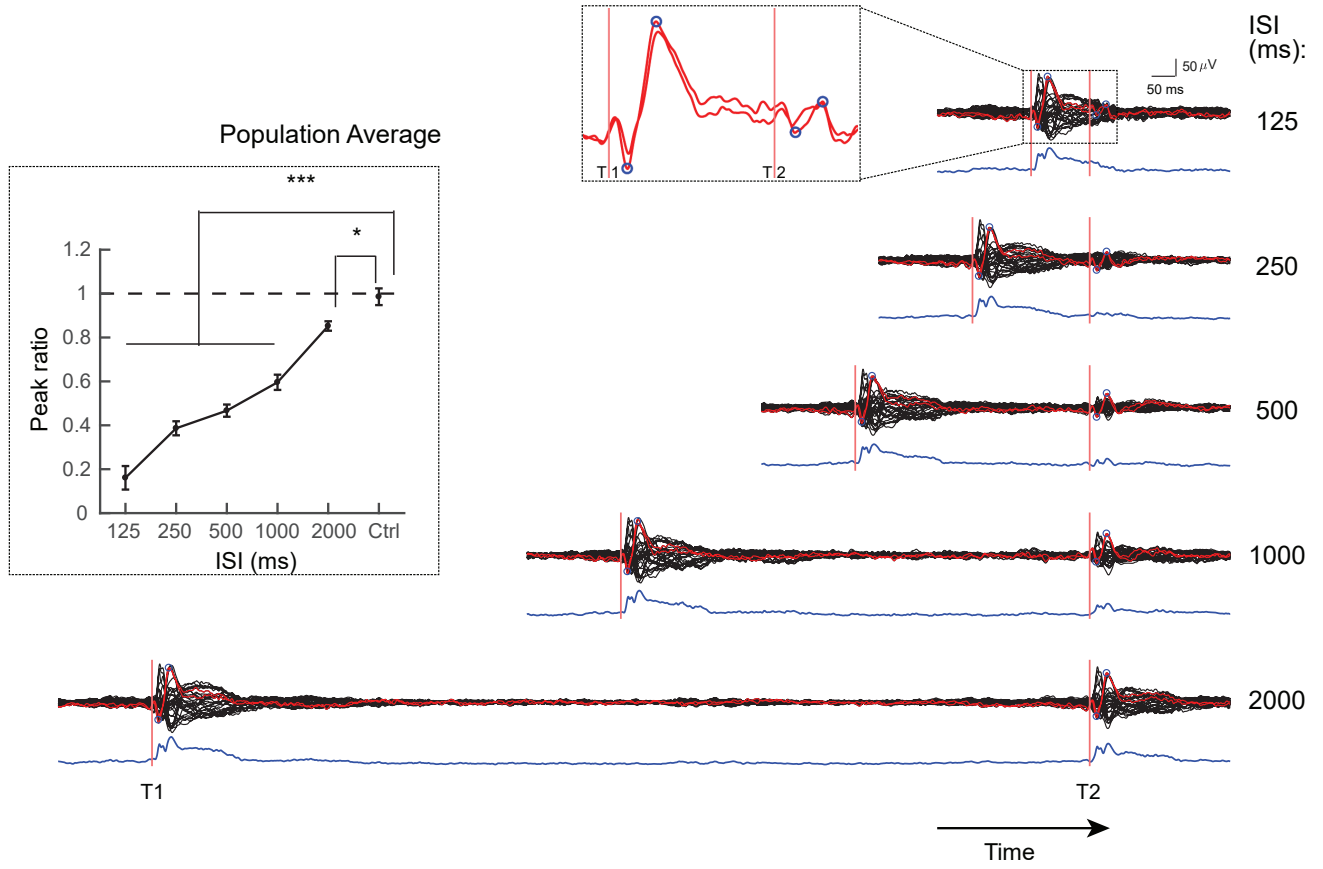
774 **Figure 8:** Auditory sensory gating at ventral cochlear nucleus (vCN)

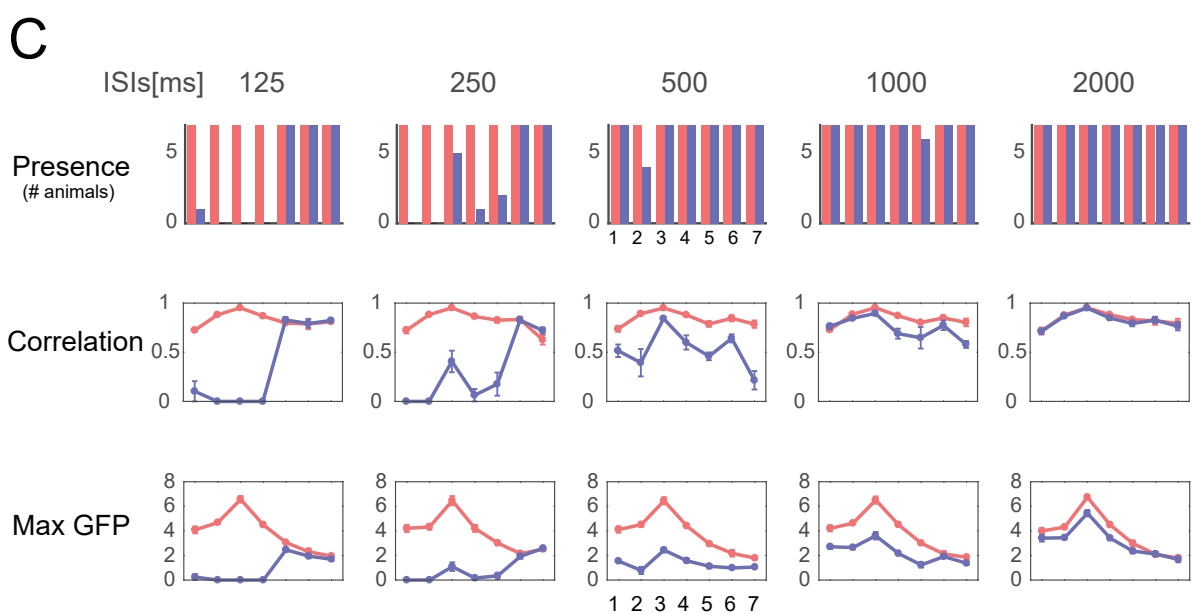
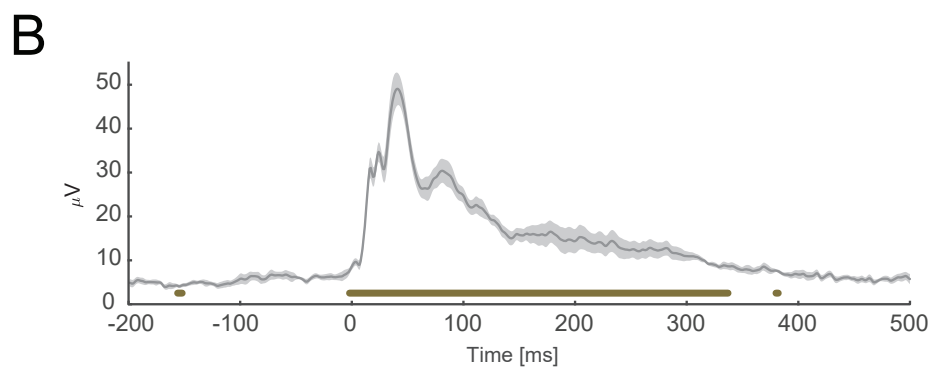
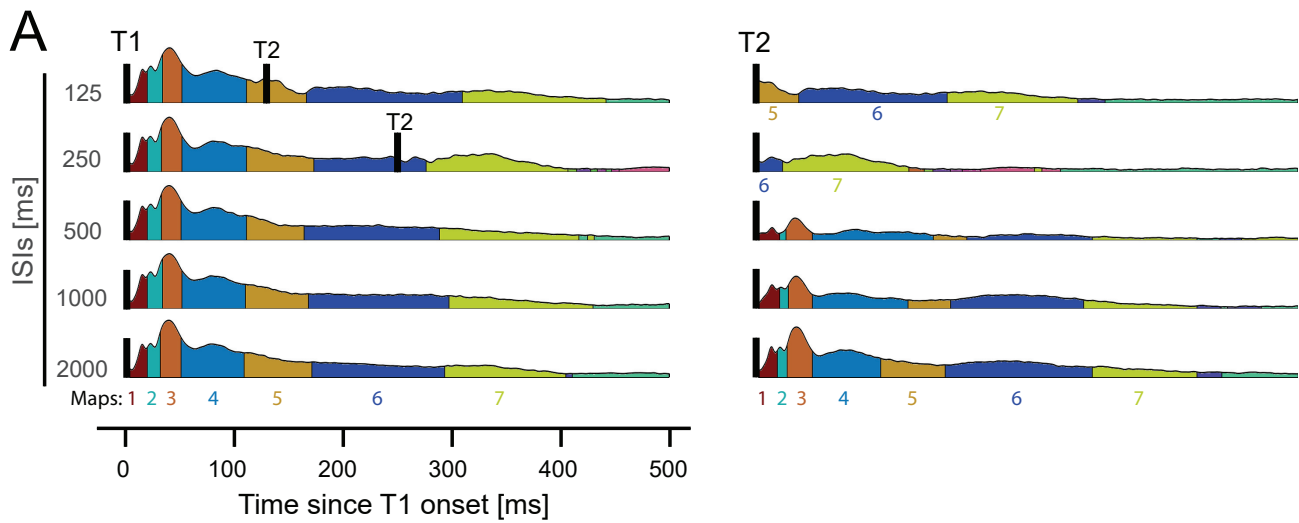
775 **A)** Illustrates the grand average ERP during ISI of 500 ms recorded from the vCN of four

776 animals. **B)** Shows auditory sensory gating (T2/T1 ratio) across different ISIs.

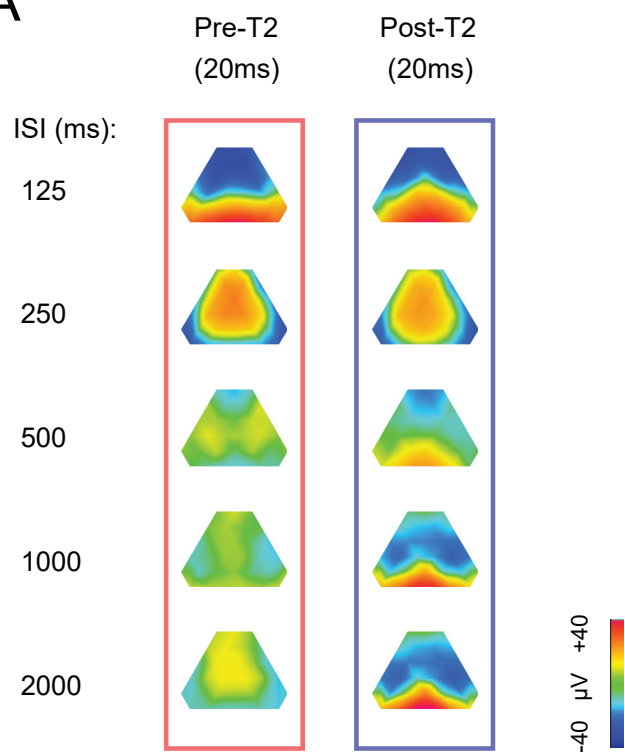


AEPs in response to paired-tone of an example subject





**A**



**B**

